



## Malaria Blood Cell Image Classification using Transfer Learning with Fine-Tune ResNet50 and Data Augmentation

Aris Muhandisin<sup>1</sup>, Yufis Azhar<sup>2</sup>

<sup>1,2</sup>Informatics, Faculty of Engineering, University of Muhammadiyah Malang

<sup>1</sup>muhandisin61@gmail.com, <sup>2</sup>yufis@umm.ac.id\*

### Abstract

Based on the WHO Report related to malaria, it is estimated that there will be 241 million malaria cases and 627,000 deaths from this disease globally in 2020 with the number of deaths increasing yearly. Preventing malaria disease conditions is through early detection. A more quick and precise malaria diagnosis method was required to simplify and reduce the detection process. Medical image classification could be carried out rapidly and precisely using machine learning or deep learning techniques. This research aims to diagnose malaria by classifying images of malaria blood cells using Deep Learning with a Transfer Learning approach. By utilizing various fine-tuning procedures and implementing data augmentation proposed method develops the method from previous studies. Two types of models Frozen ResNet50 and Fine-Tune ResNet50 are being tested. The dataset utilized will be augmented to improve model performance. This study makes use of the "NIH Malaria Cell Images Dataset" a dataset that contains a total of 27,660 image data. It is divided into two classes: parasitized and uninfected. The results are improved from previous research using the fine-tuned VGG16 model with an accuracy of 96% compared to this study using the fine-tuned ResNet50 model which achieved an accuracy score of 98%.

*Keywords:* Malaria, Image Classification, Convolutional Neural Network, Fine-Tuning, ResNet50

### 1. Introduction

Plasmodium parasites infect female Anopheles mosquitoes and then cause an acute febrile illness that can be transmitted to humans and is known as malaria. *P. falciparum* and *P. vivax* are the two parasite species that cause malaria in humans out of five parasite species [1]. According to predictions from the WHO report on malaria, there will be 241 million cases of the disease worldwide in 2020 and 627,000 fatalities from it, with the number of deaths continuing to rise yearly [2]. Meanwhile, in Indonesia, according to the Indonesian Ministry of Health, the province with the most malaria cases in Indonesia is Papua, where there were 86,022 cases reported in 2021 [3].

The best method to prevent malaria disease conditions is early detection and treatment. The most reliable and widely used method for the diagnosis of malaria continues to be the thick or thin blood smear examination [4]. A blood smear examination is used to diagnose malaria disease and produces reliable results. Parasites in blood samples will be more easily recognized and detected during the Giemsa staining procedure. Red blood cells (RBCs) and Plasmodium

parasites are stained with Giemsa. A staining object is required to detect Plasmodium parasites [5].

As the development of computer vision progresses by implementing machine learning or deep learning methods, they can be used to classify medical images quickly and accurately [6]. Canonically, image classification with machine learning approaches such as Naive Bayes, Decision Tree, Linear Discriminant, Support Vector Machine (SVM), and K-Nearest Neighbor (K-NN) has been widely used in general for malaria classification [7][8][9][10][11]. However, the challenge of using machine learning is the suitability of selecting the type of feature extraction. Color, shape, and texture, along with all their derived aspects, are among the selected features. Therefore, the success of recognition will be determined by the appropriate choice of features [12][13].

Currently, deep learning is an alternative method to perform automatic feature extraction at the initial layer of the network and capture various primitive features well [14]. Deep learning has been used in research on image classification, specifically blood smears containing malaria-infected cells. Previous research used a Convolutional Neural Network (CNN) VGG16

to classify images of malaria disease with an accuracy of 92% for Frozen VGG16 and 96% for fine-tuned VGG16 [15]. There are also similar classification problems using the same dataset, with several deep learning methods and different results [16][17][18][19]. The use of deep learning for classification also struggles to give the best results. This depends on the dataset used. The learning process in deep learning algorithms is significantly affected by the amount of data in each class. In addition, the choice of hidden layers, convolutional layer models, and other CNN parameters have a huge impact on the accuracy of results [20].

A. S. B. Reddy and D. S. Juliet published the first article utilizing Transfer Learning ResNet50 for diagnosing malaria [21]. Transfer Learning-based classification has demonstrated relatively high performance for medical image classification over the past few years. This research contributes to developing previous research [15] [21]. Utilizing an identical dataset with the addition of data augmentation techniques to help optimize the proposed method, which is a shortcoming in this study. A ResNet50 model to classify malaria blood cell images with accuracy and evaluation metrics values in comparison to previous research methods.

## 2. Research Methods

The research begins with the collection of Giemsa blood smear sample image datasets, which are then separated into three folders called train data, validation data, and test data. Details of the research stages are shown in Figure 1.

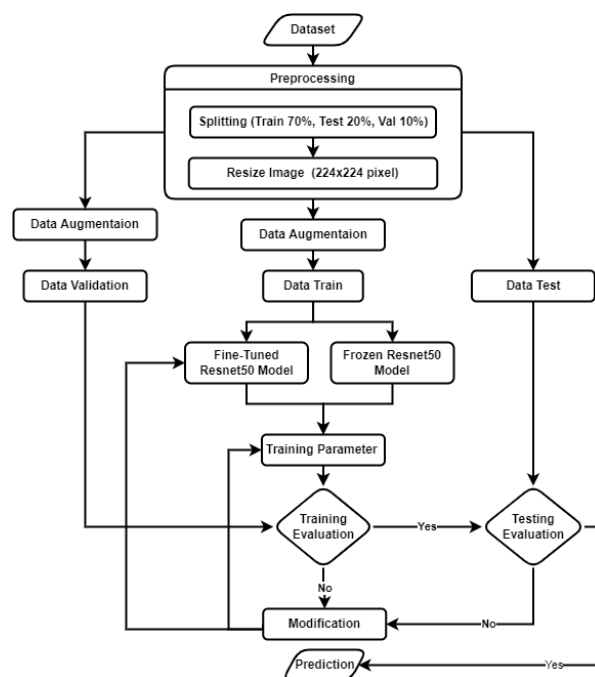


Figure 1. Research Stages

Next, change the resolution of each image in the dataset. The last stage in data preprocessing is performing data

augmentation. After the data preprocessing stage, the processing of data grouping results will continue. The train data and validation data will be used to train the model, and the test data will be used to validate the test results with the specified model and parameters.

Evaluating the Fine-Tuned Resnet50 model architecture which involves going into the modification flow by implementing various training parameters and model architecture between the two types of models if there is still no appreciable improvement in model performance from Frozen Resnet50.

### 2.1 Dataset

The dataset being used is a dataset originating from kaggle.com [22] entitled "Malaria Cell Images Dataset" which is a dataset sourced from the National Institute of Health (NIH) [23].

Within this dataset, there are two class categories, namely Parasitized and Uninfected, where each PNG format image data has a resolution that varies between 150 x 150 pixels, and the total amount of data is 27,558 malaria blood smear image datasets. Based on Figure 2, the top 5 images are blood smear images that have been infected with malaria, while the bottom 5 images are blood smear images that are not infected with malaria.

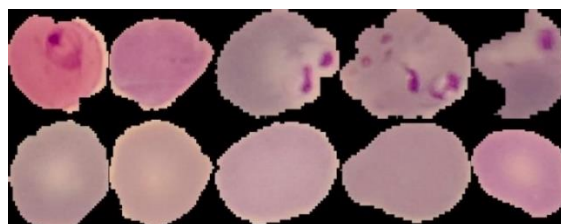


Figure 2. Images of Giemsa Malaria Blood Smears

At the Chittagong Medical College Hospital in Bangladesh, thin blood smear slides stained with Giemsa were taken from 150 *P. falciparum*-infected patients and 50 healthy patients. A slide was photographed for each minuscule field of view using the smartphone's built-in camera. The Giemsa blood smear slides image dataset has a balanced distribution of data between Parasitized and Uninfected classes. The percentage of data distribution used in this study is training by 70%, validation by 10%, and testing by 20% which is described in Table 1.

Table 1. Dataset Table

| Data       | Class       | Total |
|------------|-------------|-------|
| Train      | Parasitized | 9645  |
|            | Uninfected  | 9645  |
| Validation | Parasitized | 1378  |
|            | Uninfected  | 1378  |
| Test       | Parasitized | 2756  |
|            | Uninfected  | 2756  |

## 2.2 Data Augmentation

The data augmentation is performed by manipulating each existing image into a different form instead of adding new image variations, so the number of datasets before and after the augmentation process does not change [24][25]. The Image Data Generator is used during the augmentation process to change the shape of each image in the dataset by activating several parameters as shown in Table 2.

Table 2. Parameter Type enabled in the Data Augmentation

| Parameter                     | Value |
|-------------------------------|-------|
| featurewise_std_normalization | False |
| samplewise_std_normalization  | False |
| rotation_range                | 30°   |
| zoom_range                    | 0,3   |
| horizontal_flip               | True  |
| vertical_flip                 | False |

Ensuring that the system can still distinguish between different types of images as data for Parasitized and Uninfected classes when the classification process is performed, each image in the dataset will be partially randomly enhanced according to the activated parameters.

## 2.3. Fine-tuning

Fine-tuning refers to a technique that involves unfreezing the top few layers of the frozen base model and jointly training the newly added classifier layer and the final layer of the base model. This provides an opportunity to "fine-tune" the high-level feature representation of the base model to make it more applicable to a particular task [26].

## 2.4 Model Architecture

The Model Architecture uses a CNN model by applying the transfer learning method ResNet50, which has been fine-tuned by researchers with the addition of several layers in the top layer of ResNet50 which does not use the default top layer [27]. The proposed architecture of Fine-Tune ResNet50 can be found in Figure 3.

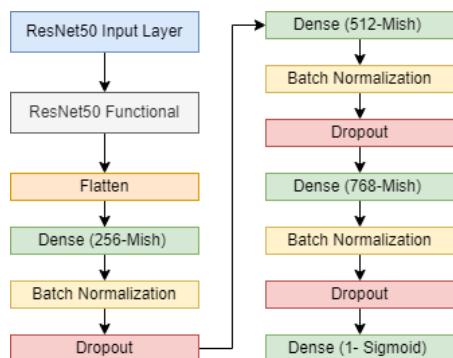


Figure 3. Fine-Tune ResNet50 model Architecture

In the fine-tuned model the weights of the initial 26 convolution blocks are frozen. The block 27 convolution and pooling block 27 convolution layers all

have trainable states. Together with the added classifier itself, all 27 block convolution layers were trained. For this model, the classifier uses 3 dense layers with 256, 512, and 768 filters with Mish activation function, for every after the first three dense layers added a Batch Normalization layer and a Dropout layer of 0.5 and an additional 1 last sigmoid dense layer.

## 2.5 Mish Activation Function

ReLU is a well-known activation function that is commonly used. In this study, the Fine-tune ResNet50 model is proposed to apply a more powerful activation function, namely Mish. The following is the mathematical definition of the Mish activation function in Equation 1 and ReLU in Equation 2 [28].

$$f(x) = x \tanh(\text{softplus}(x)) \tag{1}$$

$$f(x) = \max(0, x) \tag{2}$$

While  $\tanh()$  returns the hyperbolic tangent of a number,  $\text{softplus}()$  is a smooth approximation to ReLU and  $\max()$  determines the highest value. The self-selecting gate in the Mish activation function is considered more advantageous compared to other activation mechanisms such as ReLU with a point-to-point function. Any CNN framework can be used to implement Mish, which ensures a non-monotonic output and produces a smooth output for each point.

## 2.6 Adamax Optimizer

Adaptive Max Pooling, also known as Adamax, is an extension of the Adaptive Movement Estimation (Adam) Optimization algorithm. The Adamax optimization approach is used to improve model performance and reduce model network errors. The following are the equations of Adamax at Equation 3, Equation 4, Equation 5, Equation 6, Equation 7 [29][30].

$$m_0 = 0 \tag{3}$$

$$u_0 = 0 \tag{4}$$

$$g_t = f'(x(t-1)) \tag{5}$$

$$m_t = \beta_1 m(t-1) + (1 - \beta_1) g_t \tag{6}$$

$$u_t = \max(\beta_2 u_{(t-1)}, \text{abs}(g_t)) \tag{7}$$

Where  $m_0$  is the first momentum;  $u_0$  is the infinity norm;  $g_t$  is the gradient. The  $\text{abs}()$  function determines the absolute value and  $\max()$  selects the parameter with the highest value. The alpha value for the adamax optimizer hyperparameter or initial step size starts with  $2e-4$  [31].

## 2.7 Test Scenario

In this study, two classes will be classified, which are Parasitized and Uninfected Giemsa blood smear samples, then the dataset will be divided into three types starting from train data, validation data, and test data will be used for training and testing models. the

following are 3 main test scenarios performed with data augmentation as shown in Table 3.

Table 3. Main Test Scenario

| Model                 | Optimizer | Activation Function | Learning Rate |
|-----------------------|-----------|---------------------|---------------|
| Frozen ResNet50       | Adam      | ReLU                | 1e-4          |
| Fine-Tune ResNet50(1) | Adamax    | Mish                | 2e-4          |
| Fine-Tune ResNet50(2) | Adamax    | Mish                | 3e-4          |

### 3. Results and Discussions

The accomplished steps based on the method arrangement given in the research method constitute the findings of this study. The "Malaria Cell Images Dataset" is a dataset that includes two classes: Uninfected and Parasitized. The data is further divided into training, validation, and test data with a ratio of 70%, 10%, and 20% after being extracted from zip format. Each training, validation, and a test set of data were scaled to 224 by 224 pixels. To achieve the highest intensity for each image, the dataset is divided by 255 during the normalization procedure. Also, every image's size has been modified to a single size, and the image data is included in a single layer.

Several data augmentation techniques will be put into practice in the steps that follow randomly rotating the image by 30° due to was already sufficient for this case and rotating the image at 30° does not rotate the image at 30°, but the image is rotated randomly between 0° and 30° at each epoch. this is useful for augmentation. where each epoch, the model will be trained using a different image.

A fundamental weakness of the VGG architecture, which is the vanishing gradient problem, was one of the reasons ResNet50 was implemented. By examining the accuracy validation graph from the previous study [15], there is a less stable upward and downward trend. The vanishing gradient problem is addressed by the ResNet design. Also, VGG is slower than the more modern ResNet architecture, which incorporates the concept of residual learning and is a considerable improvement.

To find out the effect of data augmentation, an attempt we also made to test using the best method, Fine-Tune ResNet50(2) model without data augmentation, which will be explained thoroughly in the next chapter.

#### 3.1 Model Performance Comparison

Furthermore, the Resnet50 model that has been made will be run with the loss\_binary cross-entropy parameter because it only has two classes, with a batch size of 20, and 100 epochs. After the training process, the Frozen and Fine-Tune Resnet50 models with different parameters produce differences in model accuracy and the results are in Table 4.

Table 4. Accuracy Score of Each Scenario

| Model                 | Accuracy   |
|-----------------------|------------|
| Frozen ResNet50       | 96%        |
| Fine-Tune ResNet50(1) | 97%        |
| Fine-Tune ResNet50(2) | <b>98%</b> |

From the experiments conducted, all models with higher learning rates have better accuracy values, but there are different parameter usages. The use of the Adamax optimizer with the Mish activation function and an increase in the learning rate in the fine-tuned model led to an increase in the accuracy value of the Frozen Resnet50 by 2%.

Based on the results of the classification report, each experiment has different precision and recall values between classes. In Table 5, the precision value of Fine-Tuned Resnet50 with a higher learning rate has an average increase in precision and recall value of 1% compared to the Frozen Resnet50 model with a lower learning rate when correctly predicting the Parasitized class among the Uninfected class.

Table 5. Table of Precision and Recall Values for Each Scenario

| Model                 | Class       | Precision  | Recall     |
|-----------------------|-------------|------------|------------|
| Frozen ResNet50       | Parasitized | 97%        | 95%        |
|                       | Uninfected  | 95%        | 97%        |
| Fine-Tune ResNet50(1) | Parasitized | 98%        | 96%        |
|                       | Uninfected  | 96%        | 98%        |
| Fine-Tune ResNet50(2) | Parasitized | <b>99%</b> | 97%        |
|                       | Uninfected  | 97%        | <b>99%</b> |

Since the results of some of the metrics to be presented from Fine-Tuned ResNet50(1) are not appreciably different from Fine-Tuned ResNet50(2), it is considered not to be discussed further. Frozen Resnet50 model training process shows the loss and accuracy plot results listed in Figure 4 and Figure 5. Following the training process of Frozen ResNet50 showing results obtained by loss plot show the continuous linear increase in each epoch with a val\_accuracy value of 96.09% and a val\_loss that is already quite low.

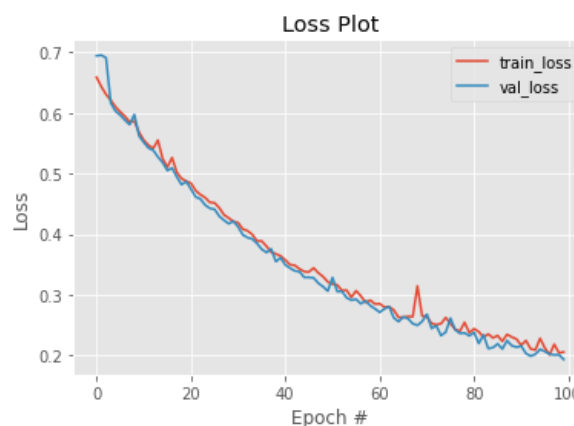


Figure 4. Loss plot for Frozen ResNet50.

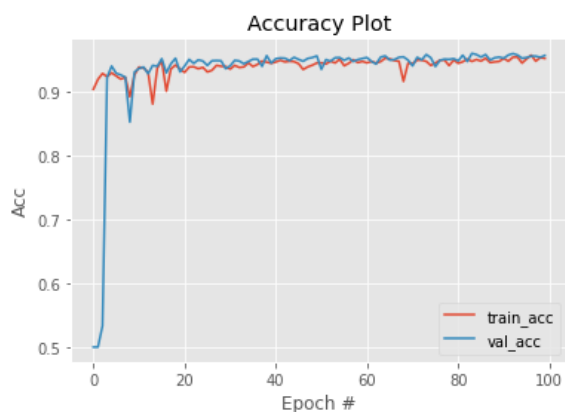


Figure 5. Accuracy plot for Frozen ResNet50.

Table 6 below is the result of the test model without and with Data Augmentation from method Fine-Tune ResNet50(2). A model with Augmented data can gaining more 2% higher results in precision and recall values compared to the without augmentation.

Table 6. Table of Precision and Recall Values for Effect of Data Augmentation in model performance Fine-Tune ResNet50(2)

| Data Augmentation | Class       | Precision  | Recall     |
|-------------------|-------------|------------|------------|
| Disabled          | Parasitized | 99%        | 95%        |
|                   | Uninfected  | 95%        | 99%        |
| Enabled           | Parasitized | 99%        | <b>97%</b> |
|                   | Uninfected  | <b>97%</b> | 99%        |

The following figures 6 and 7 show the training result plots of Fine-Tune ResNet50(2) without the data augmentation process. The loss and accuracy plots demonstrate severe overfitting conditions, particularly in the loss plot where the val\_loss and train loss values have a gap that is quite visibly present between epochs 30 to 100. The result of val\_accuracy is 96.95%, while train\_accuracy is higher at 99.75% at the 100th epoch which is probably the highest among all methods that use data augmentation, and val\_loss is also higher than train loss.

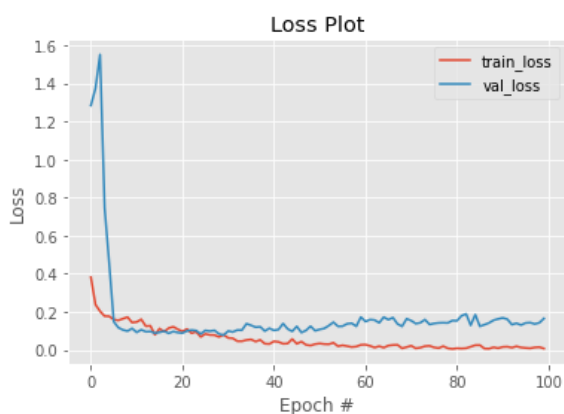


Figure 6. Loss plot Fine-Tune ResNet50(2) Without Data Augmentation.

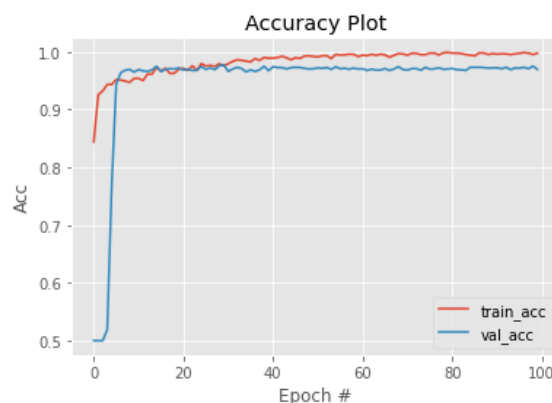


Figure 7. Accuracy plot Fine-Tune ResNet50(2) Without Data Augmentation.

Figures 8 and 9 show the loss value and accuracy results of Fine-Tune ResNet50(2) with the Data Augmentation in best fit condition than the same model or method without Data Augmentation shown before, also the accuracy plot is more stable than the Frozen ResNet50 model. The resulting val\_accuracy value is 97.60% with a relatively low val\_loss value.

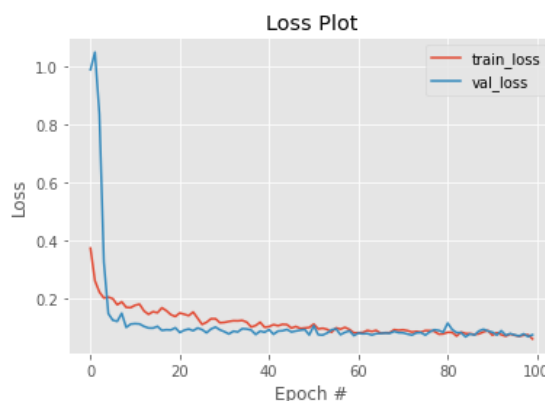


Figure 8. Loss plot for Fine-Tune ResNet50(2).

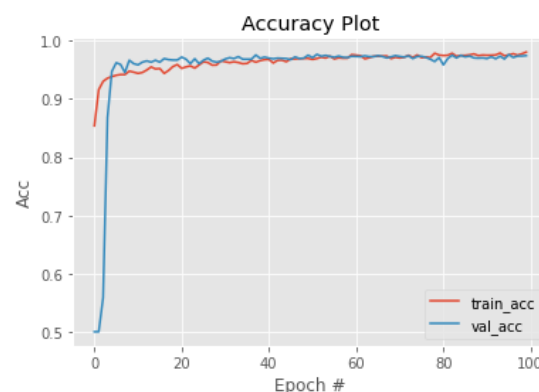


Figure 9. Accuracy plot for Fine-Tune ResNet50(2).

Finally, Figure 10 shows that the ROC curve generated by the Fine-Tuned ResNet50(2) model is better than the Frozen ResNet50. This is evidenced by the fine-tuned ResNet50(2) ROC curve is closer to a sensitivity value of 1 and a higher specificity value.

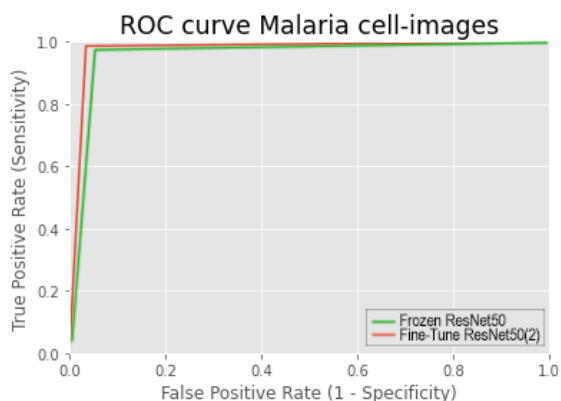


Figure 10. ROC curve for Frozen ResNet50 and Fine-Tune ResNet50(2).

After carrying out the above 3 experiments, the use of a higher learning rate with activation function Mish in the Fine-Tuned ResNet50 model performed better than the Frozen ResNet50 model. This can be proven by the decrease in val\_loss value in the Fine-Tune ResNet50(2) model and val\_accuracy, which always increases in both fine-tuned models.

### 3.2 Confusion Matrix

To evaluate the effectiveness of the developed classification method, the confusion matrix is used as the classification evaluation. The confusion table shown in Figure 11 is generated by Frozen ResNet50. From the figure, it is obvious that there are 2628 correctly predicted image data and 128 incorrectly predicted image data in the Parasitized class. In addition, 2669 image data points from the Uninfected class were correctly predicted by the model, while 87 image data points from this class were incorrectly predicted.

| Frozen ResNet50 |             |                  |            |
|-----------------|-------------|------------------|------------|
| True Labels     | Parasitized | 2628             | 128        |
|                 | Uninfected  | 87               | 2669       |
|                 |             | Parasitized      | Uninfected |
|                 |             | Predicted Labels |            |

Figure 11. Confusion matrix of Frozen ResNet50

| Fine-Tune ResNet50(2) |             |                  |            |
|-----------------------|-------------|------------------|------------|
| True Labels           | Parasitized | 2661             | 95         |
|                       | Uninfected  | 38               | 2718       |
|                       |             | Parasitized      | Uninfected |
|                       |             | Predicted Labels |            |

Figure 12. Confusion matrix of Fine-tune ResNet50(2)

The confusion matrix results of Fine-Tune ResNet50(2) are then shown in Figure 12. The confusion matrix

below shows that the Parasitized class correctly predicts 2661 image data points, while 95 image data points are wrongly predicted. For the Uninfected class, there are 2718 correctly predicted image data and 38 incorrectly predicted image data.

### 3.3 Performance Comparison of the Best Model with previous research

After performing several sets of test scenarios, the next step is to compare the performance of the best model with the results of the accuracy values obtained in previous studies. Based on Figure 13, the classification report on the Fine-Tuned ResNet50(2) model uses a learning rate of  $3e-4$  where it obtains an accuracy value of 98% and 99% precision in the Parasitized at class 0 and 97% for the Uninfected at class 1.

|              | precision | recall | f1-score | support |
|--------------|-----------|--------|----------|---------|
| 0            | 0.99      | 0.97   | 0.98     | 2756    |
| 1            | 0.97      | 0.99   | 0.98     | 2756    |
| accuracy     |           |        | 0.98     | 5512    |
| macro avg    | 0.98      | 0.98   | 0.98     | 5512    |
| weighted avg | 0.98      | 0.98   | 0.98     | 5512    |

Figure 13. Classification report for the Fine-Tune ResNet50(2)

Table 7 below describes the results of research that produced the Fine-Tune ResNet50(2) model as the best model, where this model can exceed the accuracy of the Fine-Tune VGG19 [15] model in previous studies by 2%, Frozen VGG16 [15] by 6% and for ResNet50[21] by 3% with the different fine-tuning procedure.

Table 7. Accuracy Score of Each Scenario

| Model                     | Dataset     | Accuracy   |
|---------------------------|-------------|------------|
| Frozen VGG16[15]          | NIH Malaria | 92%        |
| ResNet50[21]              | NIH Malaria | 95%        |
| Our Frozen ResNet50       | NIH Malaria | <b>96%</b> |
| Fine-Tune VGG19[15]       | NIH Malaria | 96%        |
| Our Fine-Tune ResNet50(2) | NIH Malaria | <b>98%</b> |

## 4. Conclusion

After conducting all stages of the research, it can be concluded that in the case of malaria disease image classification by utilizing data augmentation techniques described above to optimize ResNet50 in the Frozen model shows a good accuracy value of 96%. However, by performing a fine-tuning procedure using the Mish activation function with the Adamax optimizer and adjusting the learning rate, the accuracy increased by 2% also the data augmentation is proven to reduce overfitting conditions. For more comprehensive testing, different gradient descent optimization, such as Nadam or SGD, can be utilized to improve model performance, allowing for the possibility of additional study. Although several variables, such as the epochs, frequency validation, and batch size, are configurable. Some suggestions above are aimed to achieve better accuracy results.

## Reference

- [1] P. M. Sharp, L. J. Plenderleith, and B. H. Hahn, "Ape Origins of Human Malaria," *Annu. Rev. Microbiol.*, vol. 74, p. 39, Sep. 2020, doi: 10.1146/ANNUREV-MICRO-020518-115628.
- [2] "World malaria report 2021." (accessed Jul. 11, 2022).
- [3] "Sebanyak 94.610 Kasus Malaria Terjadi di Indonesia pada 2021 | Databoks." (accessed Jul. 11, 2022).
- [4] "CDC - Parasites - Malaria." (accessed Jul. 11, 2022).
- [5] K. Roy, S. Sharmin, R. B. Mufiz Mukta, and A. Sen, "Detection of Malaria Parasite in Giemsa Blood Sample Using Image Processing," *Int. J. Comput. Sci. Inf. Technol.*, vol. 10, no. 1, pp. 55–65, Oct. 2018, doi: 10.5121/IJCSIT.2018.10105.
- [6] L. Cai, J. Gao, and D. Zhao, "A review of the application of deep learning in medical image classification and segmentation," *Ann. Transl. Med.*, vol. 8, no. 11, pp. 713–713, Jun. 2020, doi: 10.21037/ATM.2020.02.44.
- [7] P. K. Maduri, Shalu, S. Agrawal, A. Rai, and S. Chaubey, "Malaria Detection Using Image Processing and Machine Learning," *Proc. - 2021 3rd Int. Conf. Adv. Comput. Commun. Control Networking, ICAC3N 2021*, pp. 1789–1792, Jan. 2018, doi: 10.48550/arxiv.1801.10031.
- [8] N. Abbas *et al.*, "Plasmodium life cycle stage classification based quantification of malaria parasitaemia in thin blood smears," *Microsc. Res. Tech.*, vol. 82, no. 3, pp. 283–295, Mar. 2019, doi: 10.1002/JEMT.23170.
- [9] M. Poostchi, K. Silamut, R. J. Maude, S. Jaeger, and G. Thoma, "Image analysis and machine learning for detecting malaria," *Transl. Res.*, vol. 194, p. 36, Apr. 2018, doi: 10.1016/J.TRSL.2017.12.004.
- [10] Muhathir, R. A. Rizal, J. S. Sihotang, and R. Gultom, "Comparison of SURF and HOG extraction in classifying the blood image of malaria parasites using SVM," *2019 Int. Conf. Comput. Sci. Inf. Technol. ICoSNIKOM 2019*, Nov. 2019, doi: 10.1109/ICOSNIKOM48755.2019.9111647.
- [11] R. Malhotra, D. Joshi, and K. Y. Shin, "Approaching Bio Cellular Classification for Malaria Infected Cells Using Machine Learning and then Deep Learning to compare & analyze K-Nearest Neighbours and Deep CNNs," May 2020, Accessed: Jul. 11, 2022. [Online]. Available: <http://arxiv.org/abs/2005.11417>
- [12] S. C. Kalkan and O. K. Sahingoz, "Deep learning based classification of malaria from slide images," *2019 Sci. Meet. Electr. Biomed. Eng. Comput. Sci. EBBT 2019*, Apr. 2019, doi: 10.1109/EBBT.2019.8741702.
- [13] Vijayalakshmi A and Rajesh Kanna B, "Deep learning approach to detect malaria from microscopic images," *Multimed. Tools Appl.* 2019 7921, vol. 79, no. 21, pp. 15297–15317, Jan. 2019, doi: 10.1007/S11042-019-7162-Y.
- [14] S. Rajaraman *et al.*, "Pre-trained convolutional neural networks as feature extractors toward improved malaria parasite detection in thin blood smear images," *PeerJ*, vol. 6, no. 4, 2018, doi: 10.7717/PEERJ.4568.
- [15] G. Shekar, S. Revathy, and E. K. Goud, "Malaria Detection using Deep Learning," *Proc. 4th Int. Conf. Trends Electron. Informatics, ICOEI 2020*, pp. 746–750, Jun. 2020, doi: 10.1109/ICOEI48184.2020.9143023.
- [16] A. Maqsood, M. S. Farid, M. H. Khan, and M. Grzegorzec, "Deep Malaria Parasite Detection in Thin Blood Smear Microscopic Images," *Appl. Sci.* 2021, Vol. 11, Page 2284, vol. 11, no. 5, p. 2284, Mar. 2021, doi: 10.3390/AP11052284.
- [17] T. Fatima and M. S. Farid, "Automatic detection of Plasmodium parasites from microscopic blood images," *J. Parasit. Dis.* 2019 441, vol. 44, no. 1, pp. 69–78, Sep. 2019, doi: 10.1007/S12639-019-01163-X.
- [18] Y. M. Kassim, F. Yang, H. Yu, R. J. Maude, and S. Jaeger, "Diagnosing Malaria Patients with Plasmodium falciparum and vivax Using Deep Learning for Thick Smear Images," *Diagnostics* 2021, Vol. 11, Page 1994, vol. 11, no. 11, p. 1994, Oct. 2021, doi: 10.3390/DIAGNOSTICS11111994.
- [19] E. T. Efaz, F. Alam, and M. S. Kamal, "Deep cnn-supported ensemble cadx architecture to diagnose malaria by medical image," *Adv. Intell. Syst. Comput.*, vol. 1309, pp. 231–243, 2021, doi: 10.1007/978-981-33-4673-4\_20/COVER/.
- [20] A. E. Minarno, Y. Azhar, F. D. Setiawan Sumadi, and Y. Munarko, "A Robust Batik Image Classification using Multi Texton Co-Occurrence Descriptor and Support Vector Machine," *2020 3rd Int. Conf. Intell. Auton. Syst. ICoIAS 2020*, pp. 51–55, Feb. 2020, doi: 10.1109/ICOIAS49312.2020.9081833.
- [21] A. Sai Bharadwaj Reddy and D. Sujitha Juliet, "Transfer learning with RESNET-50 for malaria cell-image classification," *Proc. 2019 IEEE Int. Conf. Commun. Signal Process. ICCSP 2019*, pp. 945–949, Apr. 2019, doi: 10.1109/ICCSP.2019.8697909.
- [22] "Malaria Cell Images Dataset | Kaggle." (accessed Jul. 12, 2022).
- [23] "LHNCBC Full Download List." (accessed Jul. 12, 2022).
- [24] P. Chlap, H. Min, N. Vandenberg, J. Dowling, L. Holloway, and A. Haworth, "A review of medical image data augmentation techniques for deep learning applications," *J. Med. Imaging Radiat. Oncol.*, vol. 65, no. 5, pp. 545–563, Aug. 2021, doi: 10.1111/1754-9485.13261.
- [25] A. Mikołajczyk and M. Grochowski, "Data augmentation for improving deep learning in image classification problem," *2018 Int. Interdiscip. PhD Work. IIPHDW 2018*, pp. 117–122, Jun. 2018, doi: 10.1109/IIPHDW.2018.8388338.
- [26] T. Jameela, K. Athotha, N. Singh, V. K. Gunjan, and S. Kahali, "Deep Learning and Transfer Learning for Malaria Detection," *Comput. Intell. Neurosci.*, vol. 2022, pp. 1–14, Jun. 2022, doi: 10.1155/2022/2221728.
- [27] S. A. Elghany, M. Ramadan, M. Elmogy, M. R. Ibraheem, and M. Alruwaili, "Diagnosis of Various Skin Cancer Lesions Based on Fine-Tuned ResNet50 Deep Network", doi: 10.32604/cmc.2021.016102.
- [28] D. Misra, "Mish: A Self Regularized Non-Monotonic Activation Function," Aug. 2019, doi: 10.48550/arxiv.1908.08681.
- [29] E. M. Dogo, O. J. Afolabi, N. I. Nwulu, B. Twala, and C. O. Aigbavboa, "A Comparative Analysis of Gradient Descent-Based Optimization Algorithms on Convolutional Neural Networks," *Proc. Int. Conf. Comput. Tech. Electron. Mech. Syst. CTEMS 2018*, pp. 92–99, Dec. 2018, doi: 10.1109/CTEMS.2018.8769211.
- [30] S. Himori *et al.*, "Comparative study of optimization techniques in deep learning: Application in the ophthalmology field," *J. Phys. Conf. Ser.*, vol. 1743, no. 1, p. 012002, Jan. 2021, doi: 10.1088/1742-6596/1743/1/012002.
- [31] Z. Shi, X. Xu, X. Liu, J. Chen, and M.-H. Yang, "Video Frame Interpolation Transformer," Nov. 2021, doi: 10.48550/arxiv.2111.13817.